Surface Science 677 (2018) 99–104

Contents lists available at ScienceDirect

Surface Science

journal homepage: www.elsevier.com/locate/susc

Al rich (111) and (110) surfaces of $LaAlO_3$

Pratik Koirala, Elizabeth Steele, Ahmet Gulec, Laurence Marks*

Department of Materials Science and Engineering, Northwestern University, Evanston, IL 60208, USA

ARTICLE INFO

Keywords:
Surface reconstruction
Density functional theory
X-ray photoelectron spectroscopy
Lanthanum aluminate

ABSTRACT

Lanthanum aluminate ($LaAlO_3$) has garnered significant interests since the discovery of a 2D electron gas at the $LaAlO_3/SrTiO_3$ interface. In this work, the (110) surface of $LaAlO_3$ was studied using a combination of transmission electron microscopy plan and profile imaging, image simulation, electron diffraction, X-ray photoelectron spectroscopy, and density functional theory calculations. Profile imaging of the (110) surface was performed on a (111) oriented single crystalline sample with an Al rich surface. Our results indicate that high annealing temperatures (1000–1300 °C) commonly used in preparing well ordered, flat surfaces of $LaAlO_3$ result in Al rich surfaces. The (110) surface was found to be single layered AlO_x with a (2 × 1) reconstruction. Angle resolved X-ray photoelectron spectroscopy indicated that the (2 × 1) surface structure was not hydrated. Convex hull construction of surface enthalpies as a function of excess $AlO_{1.5}$ on the (110) surface was done using density functional theory calculations.

1. Introduction

There has been continued interest in $LaAlO_3$ (LAO) since the discovery of the 2D electron gas at the $LaAlO_3/SrTiO_3$ (STO) [001] interface [1], with high electron mobility also observed for other orientations [2]. The role of oxygen vacancies and electronic reconstructions has been studied extensively [3,4], along with surface metallicity due to adsorbates [5]. The relatively small lattice parameter of LAO (3.79 Å) compared to other perovskites [6] is also useful in strain engineering. Therefore, for fundamental understanding as well as for a wide array of applications, it is important to understand the surface composition and the detailed atomic structure of surfaces and interfaces on LAO.

Despite a significant amount of work reported in the literature on electronic applications, surface studies of LAO have mostly been qualitative [7–11] and detailed atomic structure studies sparse [12, 13]. The majority of the work on surface structure studies of perovskite oxides has focused on $SrTiO_3$ [14–22]. A previous analysis indicated the presence of Al-O termination in samples heated up to 150 °C, La-O termination at temperatures above 250 °C and mixed termination in the intermediate temperature range [11]. However, in this study the sample were initially annealed under ultra-high vacuum conditions at 800 °C and it is likely that the surface was established at 800 °C, rather than at the 150 °C or 250 °C final treatments since diffusion at these lower temperatures will be sluggish. This is consistent with another study with synchrotron X-ray radiation which showed that structural relaxations only occurred at elevated temperatures (> 400 °C) [23].

The detailed atomic structure of two surface reconstructions on LAO, the $(\sqrt{5} \times \sqrt{5})R26.6$ [13] on the pseudo-cubic (001) surface and the (3 × 1) [12] on the (110) surface, have been previously reported in the literature. (For completeness, although LAO is strictly rhombohedral the distortion from cubic is small so we will use throughout the cubic cell notation.) These reconstructions were both ordered at annealing temperatures in the range of 1100–1500 °C in oxidizing conditions. The (3 × 1) surface was found to be rich in Al with a small amount of retained water and no surface La, whereas the fractional hole $(\sqrt{5} \times \sqrt{5})R26.6$ is stoichiometric in the La/Al surface composition. There is need for more data on other surface structures to understand the surface dynamics and stabilization mechanisms in LAO; this can also provide a fundamental understanding that would be applicable to a wide range of other oxides.

In this work, primarily the pseudo-cubic (110) surface of $LaAlO_3$ was studied using a combination of transmission electron microscopy plan and profile imaging, image simulation, electron diffraction, X-ray photoelectron spectroscopy, and density functional theory calculations. Profile imaging of (110) surface was performed on a (111) oriented single crystalline sample with an Al rich surface.

2. Methods

Single crystalline substrates of (110) and (111) oriented LAO were purchased from MTI Corp. (Richmond, CA), cut into 3 mm discs using an ultrasonic cutter, polished using silicon carbide sand paper and a 18μm slurry to a thickness of 100μm, and dimpled to a thickness of

* Corresponding author.
E-mail address: l-marks@northwestern.edu (L. Marks).

https://doi.org/10.1016/j.susc.2018.05.015
Received 30 November 2017; Received in revised form 20 May 2018; Accepted 24 May 2018
Available online 23 June 2018

15μm using a Gatan 656 dimple grinder. Using a Gatan PIPS, the samples were then ion milled to electron transparency, which was determined by observation of a small hole with an optical microscope under a magnification of 20X. Samples were annealed in a quartz tube furnace in flowing dry oxygen.

Electron microscopy was performed using a Hitachi H8100 and an aberration-corrected JEOL ARM 200CF. Multislice simulations [24,25] of electron microscopy images were performed using the MacTempas code [26]. Relevant collection angles for different imaging modes are given in the image captions. X-ray photoelectron spectroscopy (XPS) was performed using a Thermo-Scientific Escalab 250Xi equipped with a monochromated Al K-alpha source. Angle resolved XPS was performed by tilting the sample stage. Using a layer by layer attenuation model [27] for integrated intensity, the relative surface composition of Al to La was obtained and normalized to the experimental data at normal incidence.

Density functional theory (DFT) calculations were performed using the all-electron augmented plane wave + local orbitals WIEN2K code [28] using the PBE [29] functional to relax atomic positions, and the TPSS functional [30] to calculate surface energies. Muffin tin radii (RMT) of 2.36 was used for La and 1.55 was used for both Al and O. An RKMAX (product of smallest atomic sphere radius (RMT) and the largest K-vector) cutoff of 7 was used with a separation of 0.1 nm^{-1} between k-points in reciprocal space. The self-consistent density and positions were converged with a parallel fixed-point algorithm [31]. All atoms positions were relaxed with a numerical precision of 0.01 eV per 1×1 surface unit cell. The relaxed slab for each structure is included in supplemental information as a Crystallographic Information File (CIF). Bond-Valence Sum (BVS) of relaxed structures were also calculated using *KDist* (part of the Kalvados program suite [32]), for an integrity cross-check on the surface structures [18].

3. Results

We will first describe the broad details of the samples and the surfaces from electron microscopy analysis followed by a description of the surface composition based upon XPS results and subsequent analysis of possible atomic configurations consistent with the electron diffraction and XPS data. Finally, we corroborate the evidence for the surface structure from direct profile imaging.

Samples of (110) oriented LAO were studied using electron microscopy after Ar^+ ion milling to electron transparency. The samples show damage after ion milling evident from the bend contours in the bright field image as well as the diffuse ring in the diffraction pattern (see Fig. 1). Half ordered spots (marked by a white arrow in Fig. 1b) originating from the distortions away from cubic to rhombohedral of the lattice are also visible in the diffraction patterns.

The samples after initial investigation were annealed in dry oxygen at 1050 – 1250 °C for 8 – 12 h in a quartz tube furnace. Bright field and dark field images in Fig. 2 show well-ordered steps and terraces on the (110) surface after annealing. The transmission electron diffraction pattern in Fig. 2c shows additional spots due to a surface structure of (2×1) periodicity. It is important to note that similar annealing temperatures can also lead to the formation of (3×1) if there was trace water present in the gas flow. It is likely that the dry annealing conditions led to the formation of a dry (2×1) surface rather than the slightly hydrated (3×1), which the XPS results shown later substantiate.

The (111) terminated LAO samples were annealed under similar conditions and temperatures as the (110) samples. Bright field and dark field transmission electron microscopy (TEM) images (see Fig. 3) show discrete thickness fringes due to steps and terraces on the surface. The electron diffraction pattern (inset in Fig. 3a) showed no extra spots indicating either the absence of a long-range order at the surface or the presence of a (1×1) surface.

Turning now to the chemical composition of the surface. XPS analysis was performed to determine the surface composition of both the (110) and (111) oriented LAO samples. For this analysis to be valid, the sample surface has to be clean. In order to ensure such a surface, XPS analysis was done right after annealing in the quartz tube furnace and the samples were degassed in the XPS chamber prior to data collection. The absence of shoulder peaks in the C1s and O1s spectra indicated a clean surface; except for low levels of adventitious carbon no impurities were detected in routine survey scans (not shown). Of particular importance is to check for any residual chemisorbed water. The intensity ratio of OH to O shows no increasing trend with increase in take-off angle, thus indicating the presence of a dry surface as shown in Fig. 4.

Al2p and La3d spectra at different grazing angles were collected for both samples. XPS take off angles are referenced with respect to the surface normal (higher angles are more surface sensitive). At small take off angles, the X-ray photoelectrons are dominated by the bulk signal. For $LaAlO_3$ at 0°, the intensity ratio of Al to La corresponds to 1:1 composition in Al to La and therefore can be used for normalization of the intensity ratio. The ratio of integrated intensities is given in Fig. 5 along with the calculated angle dependent intensity ratios for different surface compositions. (See Ref. [12,27] for details of the fitting method.) These results indicate that the (110) terminated surface has an extra $AlO_x/(1 \times 1)$ and the (111) terminated surface has $2.5AlO_x/(1 \times 1)$ in excess. The surface composition obtained from XPS provided a constraint on feasible surface structures for the (2×1) surface reconstruction. Therefore, we focus on structures with an extra $AlO_x/(1 \times 1)$ for both density functional theory calculations and subsequent

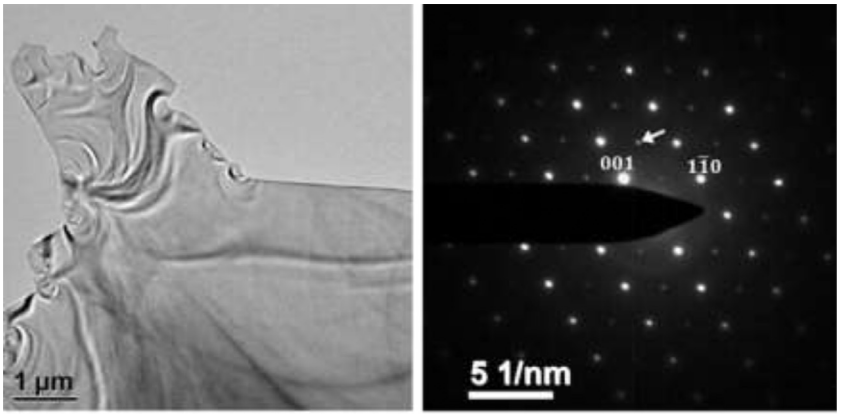

Fig. 1. Bright field transmission electron microscopy image in (a) and the corresponding electron diffraction in (b) along the [110] zone with the beam stop over the direct beam. The half-ordered spots (marked by the white arrow) in the diffraction pattern originate from distortions of the cubic to a rhombohedral cell.

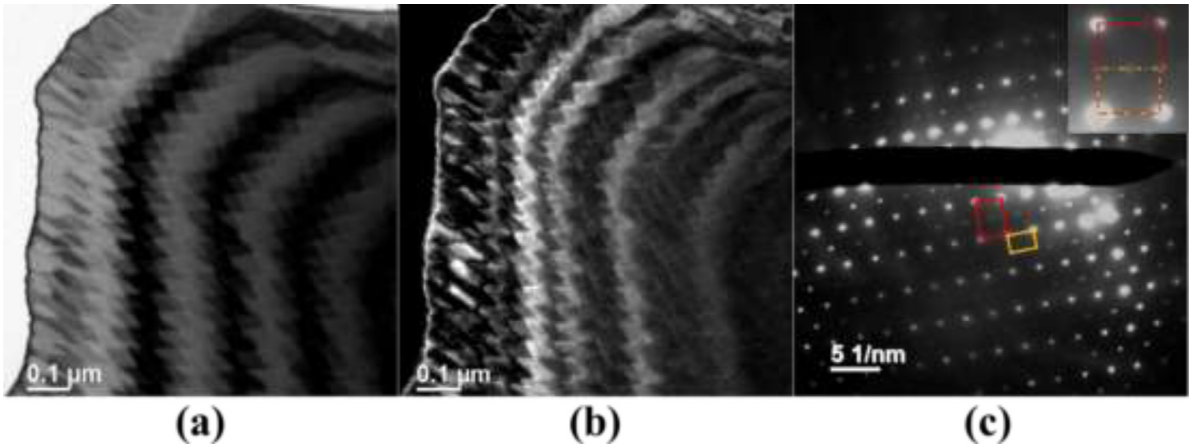

Fig. 2. Bright field and dark field transmission electron microscopy images in (a) and (b), respectively, along with the corresponding off zone diffraction pattern in (c) along [110] oriented LAO. The bulk unit cell has been outlined in red and the (2 × 1) surface unit cell has been outlined in yellow along with a magnified view of the diffraction pattern inset.

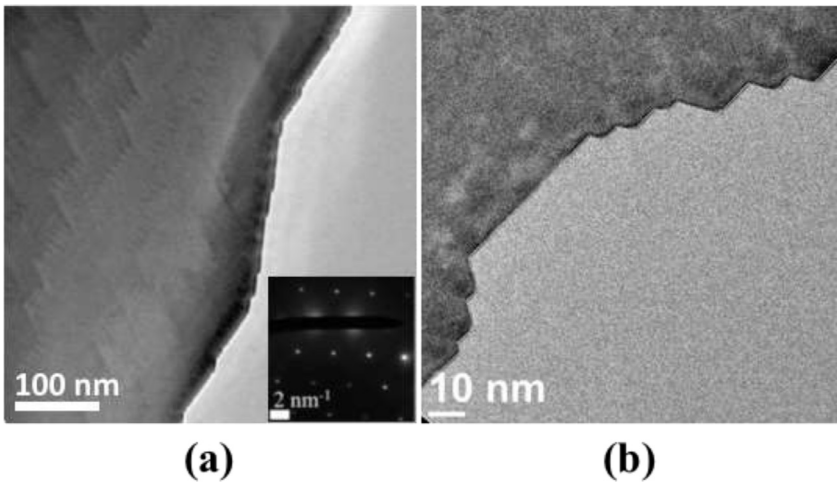

Fig. 3. Bright field images in (a) and (b) along with the corresponding off zone diffraction pattern inset along [111] oriented LAO. The lower magnification image in (a) shows discrete thickness fringes and the magnified image in (b) shows a pronounced surface layer on the [110] edge.

image simulations.

Turning now to the surface atomic structure, one Al atom per (1 × 1) unit cell on a valence neutral (110) surface was used as a constraint to identify several possible structures – there are only a few possibilities that satisfy the constraints. These structures were relaxed using DFT calculations. The surface enthalpy per (1 × 1) for each of these structures was calculated as

$$E_{surf} = \frac{E_{slab} - nE_{bulk} - mE_{AO}}{2N_{1\times 1}}$$

where n is the number of bulk unit cells in the slab, m is the number of excess Al_2O_3 on the surface, E_{slab} is the total energy of the slab, E_{bulk} and E_{AO} are the energies of bulk LAO and Al_2O_3 and $N_{1\times 1}$ is the number of (1 × 1) surface cells.

The calculated surface enthalpies were used to construct a convex hull for the (110) surface of LAO. The convex hull construction connects the minima in surface energy as a function of surface composition. Energies across different compositions cannot be compared, but thermodynamic stability for a given composition can be inferred. A number of structures previously relaxed for the (3 × 1) surface reconstruction on the (110) surface were also used in the convex hull construction [12]. Since only the (3 × 1) surface structure has been solved on the

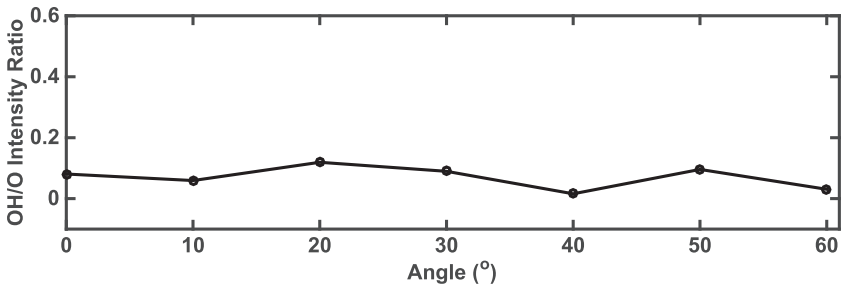

Fig. 4. Experimental angle resolved X-ray photoelectron spectroscopy intensity ratio of O1s shoulder (OH) to main (O) peak of the (110) oriented $LaAlO_3$ sample with (2 × 1) surface reconstruction.

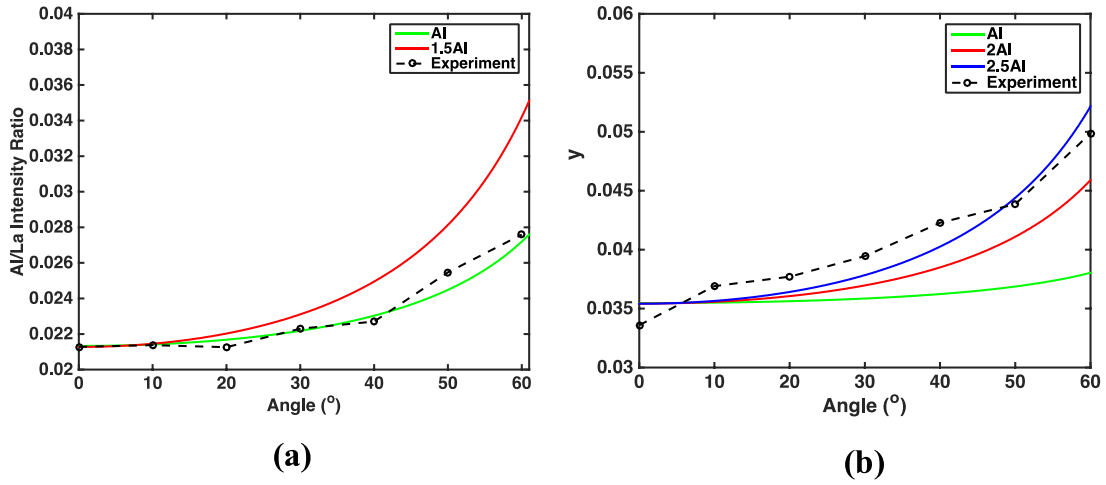

Fig. 5. Experimental angle resolved X-ray photoelectron spectroscopy intensity ratios of Al to La along with the calculated ratio using a layer by layer model in (a) the (110) LAO surface and in (b) the (111) LAO surface. The simulated intensity ratio is normalized to the experimental value at 0° at which XPS spectra is primarily comprised of the bulk signal.

Table 1
Bond valence sum of different sites on the surface and sub-surface of different DFT relaxed structure for the (2 × 1) surface reconstruction on the (110) surface of $LaAlO_3$. (Atom labels are referenced to different sites in the CIF files included in the supplementary information).

Structure	Thickness (Å)		Surface			Subsurface		
	Slab	Vacuum	Atom	BVS	Mult.	Atom	BVS	Mult.
s1	21.84	8.16	Al002	2.09	4	Al003	2.67	4
			O017	1.91	8	La010	3.19	2
			O019	1.20	2	La011	2.90	2
			O023	1.15	2	O015	2.19	2
s3	21.84	8.16	Al002	2.35	4	Al003	2.71	4
			O017	1.80	8	La010	2.97	2
			O022	1.81	4	La011	2.97	2
						O015	1.80	2
s4	22.68	7.32	Al002	2.39	4	Al003	2.56	4
			O017	1.72	8	La010	2.86	2
			O023	1.56	2	La011	3.14	2
						O015	1.67	2
						O019	1.79	2
s5	22.86	7.14	Al002	2.50	4	Al003	2.66	4
			O017	1.80	8	La010	2.69	2
			O023	1.50	2	La011	2.96	2
						O015	2.09	2
						O019	1.66	2
O-vac	18.27	11.73	O019	1.82	4	La009	2.92	2
						La010	2.96	2
						Al002	2.44	4
						O013	1.58	2
						O016	1.77	2
c(2 × 2)	22.84	7.16	Al002	2.50	4	La028	2.66	4
			Al003	2.36	4	La030	2.79	4
			O068	1.48	2	O040	2.10	2
			O069	1.57	2	O041	1.64	2
			O048	1.75	8	O056	1.68	2
			O051	1.72	8	O057	1.91	2
						Al006	2.68	4
						Al007	2.72	4

(110) LAO surface, it is difficult to accurately determine whether a structure has been sufficiently solved as the lowest point in the convex hull is not based on actual observed structures. In addition, the previously solved (3 × 1) [12] is a hydrated surface so a one to one comparison is not valid (it lies on a point in a higher-dimensional plot where chemisorbed water is also included). The convex hull construction is used as a measure of stability of the different (2 × 1) structures. Several (3 × 1) structures and a dry stoichiometric (2 × 1) are used to provide a baseline.

Among the several possible structures (see CIF in Supplemental Information) identified using the surface composition constraint for the (2 × 1) surface, the s5 structure was found to be lowest and within 0.12 eV of the convex hull. While this is not an unconditional proof, from our analysis it is the only structure that is both close enough and satisfies the experimental constraints.

In addition to surface energies, structural and chemical stability can also be inferred from bond valence sums (BVS). The values of BVS for surface and subsurface atoms for the different (2 × 1) structures are listed in Table 1. The lowest energy structure (see Supplemental Information s5.cif) has a tetrahedrally coordinated Al atom on the surface. The bond valence sum of surface Al is 2.5 and for the two-inequivalent surface O are 1.5 and 1.8, respectively. Another

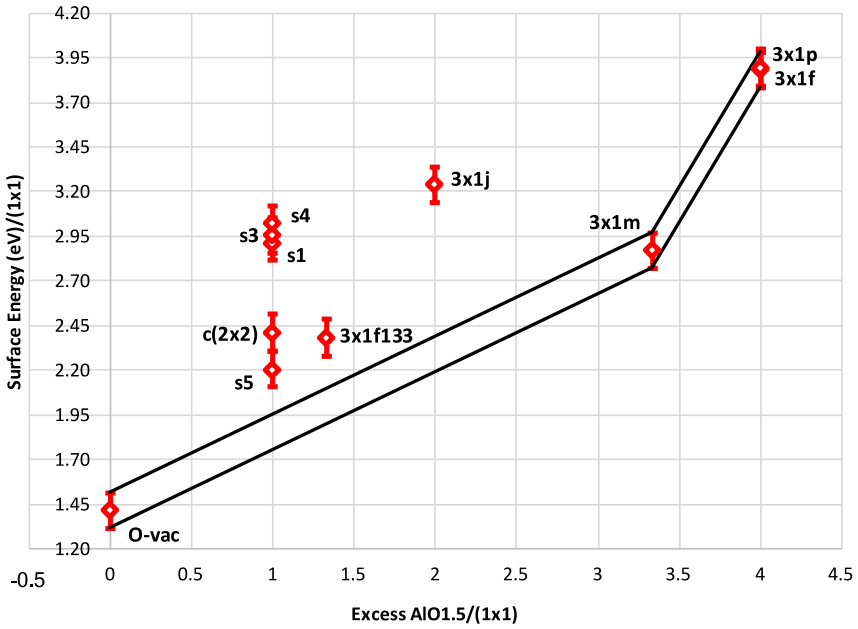

Fig. 6. DFT calculated convex hull construction of the $LaAlO_3$ (110) surface as a function of excess surface $AlO_{1.5}/(1 \times 1)$ concentration. (Deviation in the surface energy values has been marked with red error bars with error values of ± 0.1 eV.).

configuration in which the surface Al atoms are in a tetrahedral coordination was considered (see Supplemental Information s1.cif). Structure s1 achieves tetrahedrally coordinated Al at the expense of creating a sub-surface O-vac. This leads to reduction in the BVS of surface Al and O to 2.09 and 1.15–1.20, respectively, which are unreasonably small. This configuration is energetically unfavorable (0.7 eV/(1 × 1) higher than s5) as would be expected for such a reduced surface. Similarly, other configurations of Al coordinated with three surface O (s3, s4) were found to be energetically unfavorable (> 0.7 eV higher). For completeness, a centered (2 × 2) structure based on the s5 structure was also considered but was higher in energy than the s5 structure. (see energies in Fig. 6).

To cross-validate our interpretation, the (110) surface was also studied in profile view on the (111) oriented LAO samples. The (110) edge showed a distinct single layered surface structure. Annular bright field (ABF), low angle annular dark field (LAADF) and high angle annular dark field images (HAADF), with acceptance angles of 11–22 mrad, 40–90 mrad and 90–270 mrad respectively, are given in Figure 7. The probe size was 0.08 nm at our imaging conditions. The (110) edge is marked by a white arrow in images 7(a) and (b) and the corresponding magnified edge is given in 7(d) and (e). Experimental LAADF images show good contrast and periodicity of the (110) surface. As a result, LAADF images were simulated using the multislice method for comparison with experimental images using DFT relaxed structures, both s5 and O-vac.

Images simulated using the s5 and O-vac structures are given in Fig. 8b and c, along with the experimental image in 8a. Both structures provide a qualitative match with the experimental image. However, there is not enough information to discern from the experimental image whether the true structure is an oxygen vacancy driven surface ordering (O-vac) or the tetrahedrally coordinated excess surface Al since these are projection images. However, given the DFT results the s5 structure is the most probable by a significant preponderance of the evidence.

In summary, X-ray photoelectron analysis, electron microscopy imaging, image simulations and DFT calculations of surface energy were used to understand composition and structure of the (110) oriented LAO with a (2 × 1) surface reconstruction. Our results show that the (2 × 1) surface reconstruction on (110) LAO is single layered and Al rich. The convex hull construction of the 1Al per (1 × 1) surface shows that the s5-structure (see supplemental information for CIF) with

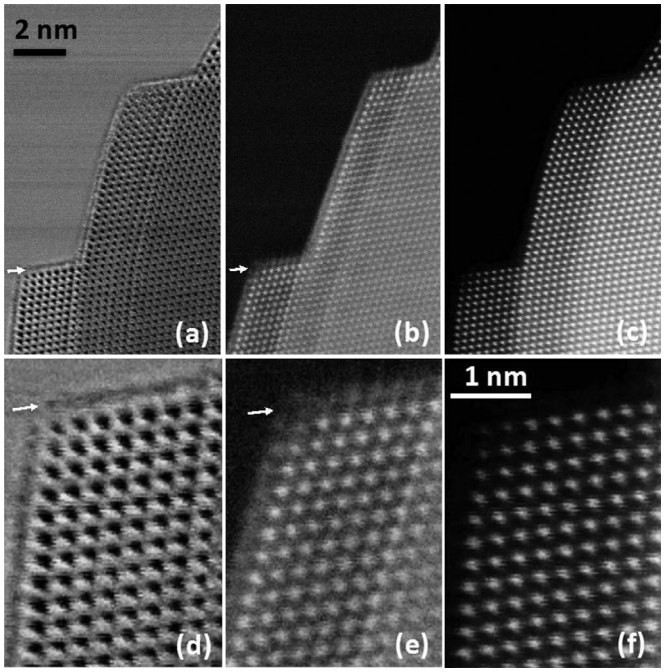

Fig. 7. (a) Annular bright field, (b) low angle annular dark field and (c) high angle annular dark field images of the edge of a sample of [111] oriented LAO. The distinct features on the (110) surface in (a) and (b) are marked with a white arrow. (d) – (f) are magnified images of edge features in (a) – (c). The acceptance angles for ABF, LAADF and HAADF were 11–22 mrad, 40–90 mrad and 90–270 mrad, respectively.

tetrahedrally coordinated Al is feasible. Profile imaging of (110) surface on the (111) oriented single crystalline sample also shows a qualitative match with the s5 structure. Understandings of surface reconstructions on $SrTiO_3$ and more recent work on rare earth scandates can be applicable to LAO, which we leave to future work.

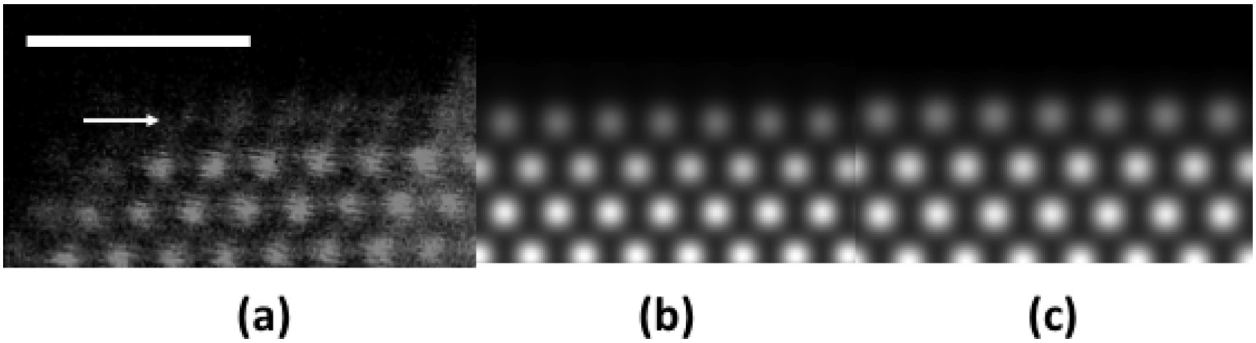

Fig. 8. Experimental low angle annular dark field image in (a) and the corresponding simulated images with electron beam along the [111] direction using structures s5 and O-vac in (b) and (c), respectively. The edge featured marked with a white arrow is the (110) surface in profile view. (The scale bar in white in (a) is 1 nm).

Acknowledgments

This work was supported by the Department of Energy on Grant Number DE-FG02 01ER45945.

Supplementary materials

Supplementary material associated with this article can be found, in the online version, at doi:10.1016/j.susc.2018.05.015.

References

[1] A. Ohtomo, H.Y. Hwang, A high-mobility electron gas at the $LaAlO_3/SrTiO_3$ heterointerface, Nature 427 (2004) 423–426.
[2] G. Herranz, F. Sanchez, N. Dix, M. Scigaj, J. Fontcuberta, High mobility conduction at (110) and (111) $LaAlO_3/SrTiO_3$ interfaces, Sci. Rep. 2 (2012) 758.
[3] M.Q. Gu, J.L. Wang, X.S. Wu, G.P. Zhang, Stabilities of the intrinsic defects on $SrTiO_3$ surface and $SrTiO_3/LaAlO_3$ interface, J. Phys. Chem. C 116 (2012) 24993–24998.
[4] X.Wang Ariando, G. Baskaran, Z.Q. Liu, J. Huijben, J.B. Yi, A. Annadi, A.R. Barman, A. Rusydi, S. Dhar, Y.P. Feng, J. Ding, H. Hilgenkamp, T. Venkatesan, Electronic phase separation at the $LaAlO_3/SrTiO_3$ interface, Nature Commun. 2 (2011) 188.
[5] W.T. Dai, S. Adhikari, A.C. Garcia-Castro, A.H. Romero, H. Lee, J.W. Lee, S. Ryu, C.B. Eom, C. Cen, Tailoring LaAlO3/SrTiO3 Interface Metallicity by Oxygen Surface Adsorbates, Nano Lett 16 (2016) 2739–2743.
[6] L.W. Martin, D.G. Schlom, Advanced synthesis techniques and routes to new single-phase multiferroics, Curr. Opin. Solid State Mater. Sci. 16 (2012) 199–215.
[7] H. Mortada, M. Derivaz, D. Dentel, J.-L. Bischoff, Structural investigation of the $LaAlO_3$(110) surface, Thin Solid Films 517 (2008) 441–443.
[8] P.A.W. van der Heide, J.W. Rabalais, Photoelectron spectroscopic study of the temperature-dependent termination of the $LaAlO_3$(100) surface, Chem. Phys. Lett. 297 (1998) 350–356.
[9] A.J.H. van der Torren, S.J. van der Molen, J. Aarts, Formation of a mixed ordered termination on the surface of LaAlO3(001), Phys. Rev. B 91 (2015) 245426.
[10] Z.L. Wang, Steps and facets on annealed $LaAlO_3$ (100) and (110) surfaces, Surf. Sci. 360 (1996) 180–186.
[11] J. Yao, P.B. Merrill, S.S. Perry, D. Marton, J.W. Rabalais, Thermal stimulation of the surface termination of $LaAlO_3$ {100}, J. Chem. Phys. 108 (1998) 1645–1652.
[12] D. Kienzle, P. Koirala, L.D. Marks, Lanthanum aluminate (110) 3×1 surface reconstruction, Surf. Sci. 633 (2015) 60–67.
[13] C.H. Lanier, J.M. Rondinelli, B. Deng, R. Kilaas, K.R. Poeppelmeier, L.D. Marks, Surface reconstruction with a fractional hole ($\sqrt{5}$ x $\sqrt{5}$)R26.6 $LaAlO_3$ (001), Phys. Rev. Lett. 98 (2007) 086102.
[14] Z. Wang, A. Loon, A. Subramanian, S. Gerhold, E. McDermott, J.A. Enterkin, M. Hieckel, B.C. Russell, R.J. Green, A. Moewes, J. Guo, P. Blaha, M.R. Castell, U. Diebold, L.D. Marks, Transition from reconstruction toward thin film on the (110) surface of strontium titanate, Nano Lett. 16 (2016) 2407–2412.
[15] A.E. Becerra-Toledo, M.R. Castell, L.D. Marks, Water adsorption on $SrTiO_3$(001): I. Experimental and simulated STM, Surf. Sci. 606 (2012) 762–765.
[16] A.E. Becerra-Toledo, J.A. Enterkin, D.M. Kienzle, L.D. Marks, Water adsorption on $SrTiO_3$(001): II. Water, water, everywhere, Surf. Sci. 606 (2012) 791–802.
[17] A.E. Becerra-Toledo, M.S.J. Marshall, M.R. Castell, L.D. Marks, c(4 × 2) and related structural units on the SrTiO3(001) surface: scanning tunneling microscopy, density functional theory, and atomic structure, J. Chem. Phys. 136 (2012) 214701.
[18] J.A. Enterkin, A.E. Becerra-Toledo, K.R. Poeppelmeier, L.D. Marks, A chemical approach to understanding oxide surfaces, Surf. Sci. 606 (2012) 344–355.
[19] A.N. Chiaramonti, C.H. Lanier, L.D. Marks, P.C. Stair, Time, temperature, and oxygen partial pressure-dependent surface reconstructions on SrTiO3(111): a systematic study of oxygen-rich conditions, Surf. Sci. 602 (2008) 3018–3025.
[20] J. Ciston, H.G. Brown, A.J. D'Alfonso, P. Koirala, C. Ophus, Y. Lin, Y. Suzuki, H. Inada, Y. Zhu, L.J. Allen, L.D. Marks, Surface determination through atomically resolved secondary-electron imaging, Nature Commun. 6 (2015) 7358.
[21] L.A. Crosby, R.M. Kennedy, B.-R. Chen, J. Wen, K.R. Poeppelmeier, M.J. Bedzyk, L.D. Marks, Complex surface structure of (110) terminated strontium titanate nanododecahedra, Nanoscale 8 (2016) 16606–16611.
[22] Y. Lin, J. Wen, L. Hu, R.M. Kennedy, P.C. Stair, K.R. Poeppelmeier, L.D. Marks, Synthesis-dependent atomic surface structures of oxide nanoparticles, Phys. Rev. Lett. 111 (2013) 156101.
[23] R. Francis, S. Moss, A. Jacobson, X-ray truncation rod analysis of the reversible temperature-dependent [001]surface structure of LaAlO3, Phys. Rev. B 64 (2001) 235425.
[24] J.M. Cowley, A.F. Moodie, The scattering of electrons by atoms and crystals. I. A new theoretical approach, Acta Crystallographica 10 (1957) 609–619.
[25] P. Goodman, A.F. Moodie, Numerical evaluations of N-beam wave functions in electron scattering by the multi-slice method, Acta Crystallographica Section A 30 (1974) 280–290.
[26] R. Kilaas, MacTempasX, http://www.totalresolution.com/, (2014).
[27] E. McCafferty, J.P. Wightman, An X-ray photoelectron spectroscopy sputter profile study of the native air-formed oxide film on titanium, Appl. Surf. Sci. 143 (1999) 92–100.
[28] P. Blaha, K. Schwarz, G. Madsen, D. Kvasnicka, J. Luitz, Wien2k, an augmented plane wave + local orbitals program for calculating crystal properties (2001).
[29] J.P. Perdew, K. Burke, M. Ernzerhof, Generalized Gradient Approximation Made Simple, Phys. Rev. Lett. 77 (1996) 3865–3868.
[30] J.M. Tao, J.P. Perdew, V.N. Staroverov, G.E. Scuseria, Climbing the density functional ladder: nonempirical meta-generalized gradient approximation designed for molecules and solids, Phys. Rev. Lett. 91 (2003) 146401.
[31] L.D. Marks, Fixed-point optimization of atoms and density in DFT, J. Chem. Theory Comput. 9 (2013) 2786–2800.
[32] K. Knížek, Kalvados - software for crystal structure and powder diffraction, in, 2012.